J Therm Anal Calorim (2016) 126:1143–1155
DOI 10.1007/s10973-016-5825-8

Factors that affect the thermal stability and properties of Zr-porous clay heterostructures

In situ studies

Fethi Kooli[1] · Yan Liu[2] · Kais Hbaieb[3] · Rawan Al-Faze[1]

Received: 16 March 2016 / Accepted: 4 September 2016 / Published online: 19 September 2016

Abstract New zirconium-porous clay heterostructures (PCHs) were prepared using zirconium-tetramer-intercalated clay mineral as precursors and a subsequent reaction with alkylamine molecules and a silica source, such as tetraethyl orthosilicate. The organic molecules were removed by calcinations at temperatures above 550 °C. The precursors and resulting materials were systematically characterized using different techniques: XRD, XRF, ^{29}Si MAS NMR, N2 adsorption, and TG-DTG. The thermal stability of the zirconium precursor and porous clay heterostructure was reported for the first time using in situ XRD high temperature. The zirconium content in the PCHs was tuned using the starting precursors with different zirconia percentages, and its presence improved the thermal stability, microtextural properties, and acidity of the PCH materials compared to the conventional PCH materials. The length of the alkyl amine chains used also affected the previously mentioned properties. A higher surface area of 950 $m^2\ g^{-1}$ and pore volume of 0.801 cc g^{-1} were obtained using dodecylamine molecules and Zr-intercalated clay with a starting ratio of Zr (mole) to grams of clay of 6. The zirconium-porous clay heterostructures were stable up to 650 °C, with a total acidity concentration of 0.993 mol g^{-1} of PCH, in addition to strong Brönsted and Lewis acid sites, which were detected at 500 °C in vacuum.

Keywords Zr-intercalated clays · Porous clay heterostructure · Thermal stability · In situ X-ray diffraction · Acidity · ^{29}Si MAS NMR

Introduction

The discovery of ordered mesoporous silica materials has attracted increasing attention because of their potential applications in many fields [1, 2]. This discovery was based on the interaction between ionic surfactants and inorganic ions, which results in an orderly mesoporous network [3]. With appropriate combinations of ionic and neutral amine-based intragallery surfactants as structure-directing agents and a neutral silicon precursor, preferably tetraethyl orthosilicate (TEOS), a silica mesostructure can be intercalated within a gallery of clay minerals, and the new material is called a porous clay heterostructure (PCHs) [4]. The PCHs exhibit interesting properties in terms of high specific surface areas and defined mesopore sizes from 1.2 to 4.0 nm [5]. These materials have been applied in different fields, such as in catalysis, the environment, biosensors and drug encapsulation [6–9]. In catalytic applications, in addition to the surface areas, acidity plays an important role and can be enhanced by different strategies, such as by using acid activated clays [10] or different types of clays as host materials [11, 12] as well as in post-synthesis and grafting of aluminum or titanium or

Electronic supplementary material The online version of this article (doi:10.1007/s10973-016-5825-8) contains supplementary material, which is available to authorized users.

✉ Fethi Kooli
fkooli@taibahu.edu.sa

[1] Department of Chemistry, Taibah University, PO Box 30002, Al-Madinah Al-Munawwarah 41411, Saudi Arabia

[2] Institute of Chemical and Engineering Sciences, 1 Pesek Road, Jurong Island 627833, Singapore

[3] Department of Mechanical Engineering, Taibah University, PO Box 441, Al-Madinah Al-Munawwarah 41411, Saudi Arabia

zirconium onto the surface of montmorillonite or saponite-derived PCH materials [13–15].

ZrO_2 is a well-known active metal oxide catalyst that is used in many chemical reactions [16]. The derived pillared clays with zirconia exhibit unusual properties compared to the clays pillared with other oxides [17]. The properties of ZrO_2-pillared clays can be tuned by varying the ZrO_2 contents [18]. The modification of PCH materials with Zr was recently reported using different Zr/Si molar ratios. Zirconium species were added to the TEOS liquid prior the synthesis of PCH precursors to produce Zr-PCH with different properties compared to conventional PCHs, which are applied in the separation of hydrocarbon mixtures [19]. The combination of the pillared process and mesoporous synthesis to prepare PCH materials that contained Al species and started from an Al_{13}-intercalated clay precursor was reported [20]. Analogously, Zr-PCH was prepared following an identical strategy from zirconium-tetramer-intercalated clay with a fixed zirconium-to-clay content [21]. In this study, the effects of different parameters on the properties of the obtained Zr-PCHs are investigated, such as the zirconium content in the starting precursors, length of the amine molecules, and calcination temperature of the PCH precursors. Different techniques were used to characterize the products. For the first time, the thermal stability of the selected precursors was performed using in situ X-ray diffraction. The acidity was investigated using cyclohexylamine and pyridine as probe molecules.

Experimental

The chemicals in the experiments were of analytical purity and used without purification. Clay montmorillonite (stx-2, Mt) was purchased from Prude University with a cation exchange capacity of 0.92 meq g^{-1}.

Preparation of Zr-intercalated clays

A series of zirconium-intercalated clays was prepared using a cation exchange reaction with a zirconyl nitrate dehydrate solution at different Zr mmole to clay ratios of 3–24 [22]. In brief, 200 mL of zirconyl nitrate dihydrate solution (0.06 M) was aged at 80 °C for 1 h, which corresponded to a Zr/clay ratio of 3 mol g^{-1}; then, 4 grams of clay in dry powder form were added to the zirconium solution and mixed for another 4 h at 80 °C. The resulting slurry was cooled at room temperature; the solid was separated by filtration and extensively and repeatedly washed with deionized water. The sample was assigned as Zr-Mt(X), where X corresponded to the Zr-mmole $clay^{-1}$ ratio.

Preparation of the Zr-PCH precursor

Effect of the Zr/clay ratio

The PCH precursor was prepared as described in our previous work [20]. One gram of the Mt-Zr(X) precursor was reacted with dodecylamine ($C_{12}H_{25}NH_2$) and TEOS at a molar ratio of clay/$C_{12}H_{25}NH_2$/TEOS of approximately 1/20/150. The mixture was stirred for 4 h at room temperature. The resulting precursor was recovered by filtration and air-dried overnight. The sample was assigned as Zr-PCH(X), for example, Zr-PCH(3) corresponds to a precursor prepared from Zr-intercalated clay at a ratio of 3, among others.

Effect of the amine length

For a selected zirconium-intercalated clay (Zr-Mt(6)), the length of the aliphatic chain in the amine molecules was varied from C_8 to C_{16}, and a similar procedure was used to prepare the corresponding PCH precursor as described in "Effect of the Zr/clay ratio" section.

Effect of the calcination temperature

The selected Zr-PCH(6) precursor was calcined in situ in an Anton Parr cell connected to an X-ray diffractometer from room temperature to 425 °C. Then, the sample was calcined in a tubular furnace in air at different temperatures of 550–900 °C to study the thermal stability of the Zr-PCH(6) material.

All of the Zr-PCH(X) precursors were calcined at a fixed temperature of 550 °C for 6 h in air to remove the amine molecules and obtain the Zr-PCH(X) materials.

Characterization methods

X-ray fluorescence (XRF) was performed to estimate the chemical composition in the metal oxide percentage of the intercalated zirconium clays and their derived PCH precursors. To confirm the success of the Zr species intercalation between clay layers and the synthesis of PCH materials, an X-ray diffractometer was used from Bruker (advance 8), which was equipped with a Ni-Filter and Cu-Kλ radiation. The in situ studies were performed using Anton Parr heating stage KT450 between room temperature and 425 °C, which was attached to the XRD diffractometer Advance8. Thermogravimetry analysis data were obtained using a TA instrument SD-966 model under a flow of air (10 mL min^{-1}) and with a heating rate of 10 °C min^{-1}. The textural characterization was performed based on the nitrogen adsorption isotherms using a Micromeritics apparatus model ASAP2020. Prior to the

measurements, the samples were treated in vacuum at 200 °C overnight. The specific surface area (SSA) was estimated using the Brunauer–Emmett–Teller (BET) method. The micropore volumes and surface areas were determined using the t-plot according to De Boer's method. The total pore volume (TPV) of the studied materials was calculated from the amount of adsorbed nitrogen at a relative pressure of 0.97. The ^{29}Si MAS (magic-angle spinning) NMR spectra were recorded on a Bruker 400 spectrometer, which operated at a ^{29}Si NMR frequency of 78 MHz. A 4-mm standard probe was used with an 8.0 kHz sample rotation rate. In total, 100 scans were performed with a recycle delay of 200 s. The ^{29}Si chemical shift is reported with respect to tetramethylsilane (TMS). The total acidity was monitored using the temperature programmed desorption (TPD) of cyclohexylamine as a probe molecule [20]. The experimental procedure was similar to that reported in our previous studies. The PCH materials were first saturated with a cyclohexylamine solution and subsequently dried at 80 °C in air to desorb the physisorbed molecules. The TPD features were recorded on TA instruments in a nitrogen atmosphere of 50 mL min^{-1} at a heating rate of 10 °C min^{-1}. The mass loss between 290 and 420 °C was computed to estimate the acidity in terms of mmol of desorbed cyclohexylamine. The pyridine molecule was used as another probe molecule to distinguish among the types of acid sites and their strength. The infrared spectroscopy of pyridine that was adsorbed onto Zr-Mt(X) and Zr-PCH(X) materials was measured in situ after the desorption of pyridine at different temperatures. The protocol was reported in our previous studies [20, 21].

Results and discussion

XRF data

The chemical compositions of different Zr-Mt(X) precursors and their derived Zr-PCH precursors are summarized in Table 1, where the major metal oxides are presented. The data indicate that calcium cations were exchanged with Zr species, and the amount of ZrO_2 (in mass) intercalated in the Zr-Mt(X) precursors depends on the starting Zr/clay ratios. The lowest value of 6.23 % was obtained for Zr-Mt(3), and the highest value of 16.70 % was obtained for the Zr-Mt(24) precursor. These data are different from those from previous study [22], where the starting Zr/clay ratios did not affect the percentage of ZrO_2 in the resulting precursors after 1 h of the exchange reaction. This difference was because of the period of time of the exchange reaction in the present study (4 h).

The decrease of SiO_2 percentage (in mass) upon increase of Zr/clay ratio is consequence of a parallel increase of ZrO_2 content. It is obvious that the more pillars in the intercalated clay, the lower the relative content of SiO_2. The experimental Zr/Clay ratios were lower than the theoretical values, as shown in Table 1, and a maximum of 1.79 was achieved.

Because the synthesis of PCH precursors is accompanied by an increase in the SiO_2 content, the latter lowers the relative amounts of non-Si elements, such as Al or Zr compared to the Zr-Mt(X) starting materials (Table 1). Similar data were reported for Al-PCH prepared from Al_{13}-intercalated clay [20]. The percentages of Zr varied from 2.36 to 5.58 %. These values are consistent with those reported in the literature for PCH precursors containing Zr species [15].

X-ray diffraction data

The powder XRD patterns of the starting Mt clay and Zr-Mt(X) precursors are shown in Fig. 1. The intensity of the first reflection was improved when the Zr/Clay ratio increased, which indicates a long-range order in these precursors, as reported in the literature [23]. The basal spacing of the starting clay was approximately 1.52 nm, which is related to the presence of calcium cations in the interlayer spacing. After the reaction with zirconyl solutions, the basal spacing expanded from 1.52 nm to higher values, depending to the starting Zr/clay ratios: it increased from 1.91 nm for Zr-Mt(3) to 2.24 nm for the Zr-Mt(24)

Table 1 Chemical analysis of major oxides (mass%) of Zr-Mt(X) and their resulting Zr-PCH(X) precursors

Samples	SiO_2	Al_2O_3	MgO	ZrO_2	CaO	Zr/clay$^+$
Mt	66.40	14.50	2.97	0.00	1.66	0.00
Zr-Mt(3)	54.50 (78.52)*	11.70 (5.53)	2.03 (1.02)	6.23 (4.21)	0.03 (0.02)	0.57
Zr-Mt(6)	49.10 (81.02)	10.40 (5.54)	1.90 (0.66)	11.00 (6.83)	0.02 (0.02)	1.12
Zr-Mt(12)	46.70 (82.21)	10.00 (5.21)	1.69 (0.62)	12.80 (7.25)	0.01 (0.02)	1.38
Zr-Mt(24)	46.40 (83.01)	9.70 (4.67)	1.65 (0.58)	16.70 (8.12)	0.00 (0.02)	1.79

* Values between brackets correspond to Zr-PCH materials. $^+$experimental values (mmole of Zr g^{-1} of clay)

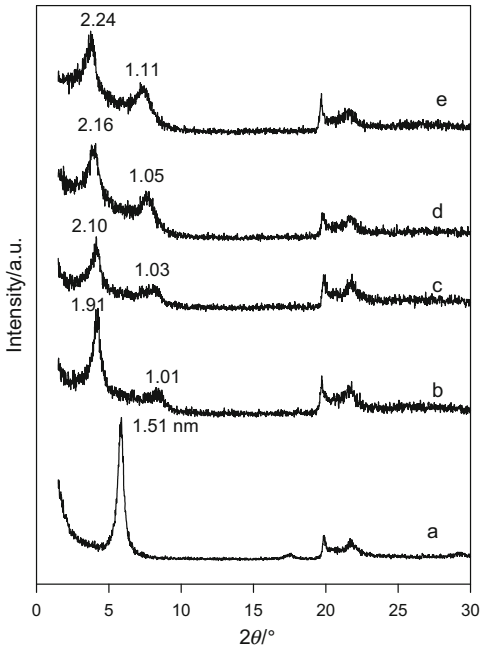

Fig. 1 Powder XRD patterns of *a* Mt clay and its zirconium-intercalated derivatives: *b* Mt-Zr(3), *c* Mt-Zr(6), *d* Mt-Zr(12) and *e* Mt-Zr(24)

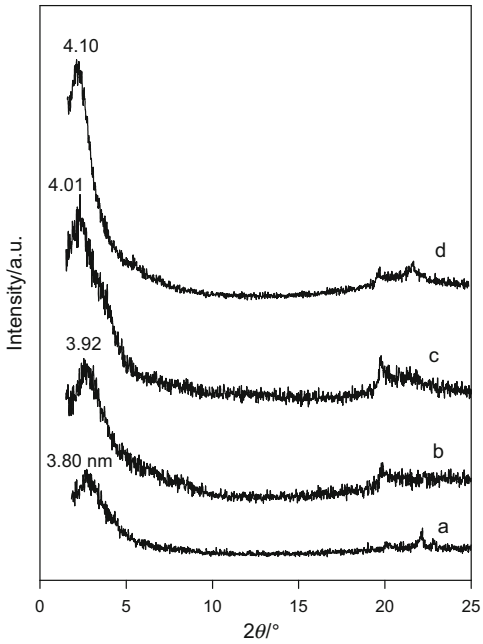

Fig. 2 Powder XD patterns of Zr-PCH(X) prepared from zirconium-intercalated clays: *a* Zr-PCH(3), *b* Zr-PCH(6), *c* Zr-PCH(12) and *d* Zr-PCH(24)

precursor. This variation is related to the ZrO_2 contents in different precursors. Similar data were reported using different starting clays and pillaring species [24, 25]. Considering that the thickness of the Mt layer is approximately 0.96 nm, the interlayer spacing of different Zr-Mt(X) precursors was in the range of 0.95–1.28 nm. The reported dimensions of Zr tetramers are 0.89 nm in width and length and 0.58 nm in thickness [26]. The condensation of tetramers occurred either lengthwise–breadthwise or thickness-wise. The average increase in interlayer space by 1.14 nm for Zr-Mt(6) precursor can be considered to be a close consistency of either double-layer flat-lying Zr tetramers or a single layer of Zr tetramer that is normal to the silicate layer [27].

After the reaction with C_{12} amine and TEOS solution, the powder XRD patterns of the Zr-PCH(X) precursors are shown in Fig. 2. The powder XRD patterns exhibited an intense reflection at lower angles, which corresponds to a basal spacing of 3.80–4.10 nm. The distance depended on the Zr contents. The PXRD patterns were similar to those reported for conventional PCH precursors with no detected multiple reflection [28]. The increase in basal spacing is related to the exchange of zirconium species with C_{12} amine cations in the first stage of the synthesis [21]. Indeed, when Zr-Mt(6) precursor was reacted with pure C_{12} amine solution, the basal spacing of the resulting material was expanded from 2.10 nm to 4.15 nm. This expansion was due to the insertion of C_{12} amine cations in the interlayer spacing [21].

The basal spacing values depend on both the ZrO_2 contents and the length of the amine chains during synthesis [5, 28]. Indeed, the Zr-PCH(6) precursor that was prepared from the Zr-Mt(6) host material exhibited different basal spacings of 3.02–4.20 nm, as shown in Fig. 3. The lowest value was obtained from C_8 amine molecules, and the highest value of 4.20 nm was achieved using C_{16} amine molecules. Similar results were reported in previous studies [17, 22, 28]. These data confirm that the formation of the Zr-PCH precursor is the result of the polymerization of silica species around the amine molecules in the interlayer spacing of the clay.

Thermal analysis and stability

A thermogravimetric analysis was used to study the thermal stability of the Zr-Mt(X) and Zr-PCH(X) precursors. The data were presented in terms of derivative thermogravimetric analysis (DTG) curves. This mathematical transformation enables us to more accurately determine the number of steps and maximum temperature of the mass loss. Figure 4 presents the TG (A) and DTG (A') curves of raw Mt and different Zr-Mt(X) precursors. Mt clay mainly exhibited one mass loss step of 10.6 % in the range of 25–200 °C (Fig. 4A) with two maximum temperatures at 71 °C and 140 °C, which are associated with water

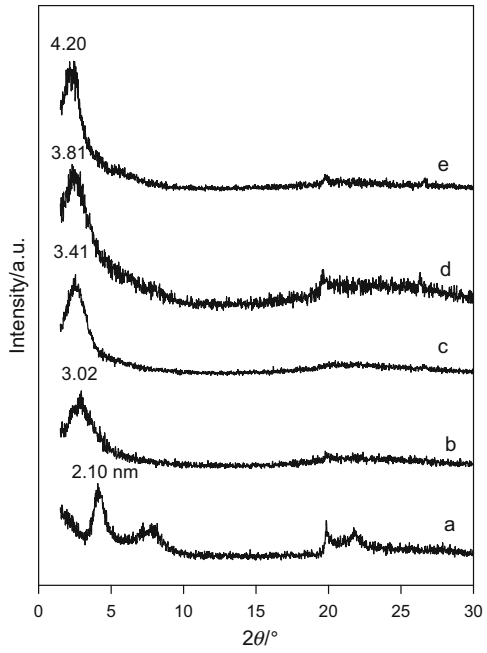

Fig. 3 Powder XRD patterns of Zr-PCH(6) prepared using TESO and different lengths of alkyl amine molecules: *a* C0, *b* C8, *c* C10, *d* C12 and *e* C16

molecules that are intercalated and coordinated to the Ca^{2+} cations (Fig. 4A'). The second mass loss of 3.01 % was related to the dehydroxylation of the clay layers in the range of 500–600 °C, with a maximum temperature mass loss at 654 °C [29]. The DTG of Zr-Mt(X) exhibited different features, particularly in the temperature range of RT to 200 °C; only one DTG peak at 70 °C was observed with a shoulder at 50 °C (Fig. 4A'), and an average mass loss of 18.2 % was observed. This value was higher to that of pure Mt (10.4 %) because of the presence of different amounts of physisorbed water molecules and was associated with the intercalated Zr tetramers between the clay layers (Fig. 4A) [30]. The mass loss at higher temperatures in the range of 500–700 °C was associated with the dehydroxylation of clay layers and Zr species with a percentage of 4–5.2 %, which is higher than that of pure Mt (3 %) (Fig. 4A) [30]. This increase was related to the presence of Zr species and its contents. The maximum temperature peak shifted to lower temperatures from 654 to 583 °C and 574 °C, which is related to the easy dehydroxylation of the clay layers (Fig. 4A'). Similar data were reported for other intercalated precursors, such as Al_{13} cations [20].

The Zr-PCH(X) precursors exhibited different TG and DTG curves from the Zr-Mt(X) host materials (Fig. 5A, A'). For example, Zr-PCH(3) exhibited two additional mass loss steps of 5 and 5.2 % in temperature range of 200–500 °C, which are assigned to the decomposition and combustion of C_{12} amine molecules with a continuous mass loss of 3 % because of the total combustion of the residual carbon materials (Fig. 5A). The decomposition was confirmed using DTG curves with three maxima temperature mass losses at 203, 329 and 470 °C (Fig. 5A') [20]. The dehydroxylation of the clay layers shifted to lower temperature at 558 °C. This shift is related to the presence of organic molecules in the precursors (Fig. 5A'). Similar data were reported for the organoclays [31]. The total mass loss associated with the C_{12} amine molecules

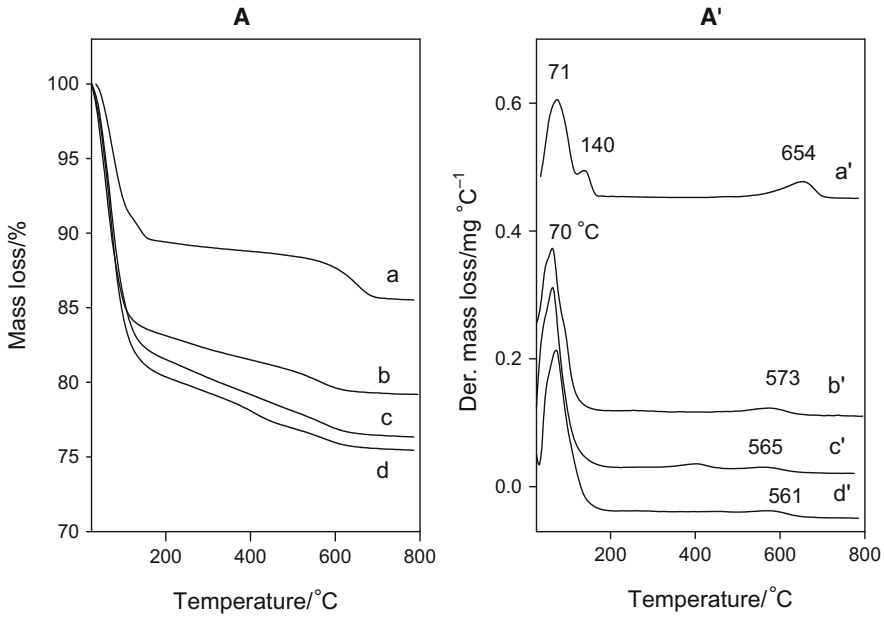

Fig. 4 TG (**A**) and DTG (**A′**) curves of *a*, *a′* raw Mt and different Zr-Mt(X) precursors: *b*, *b′* Mt-Zr(3), *c*, *c′* Mt-Zr(6), and *d*, *d′* Mt-Zr(12)

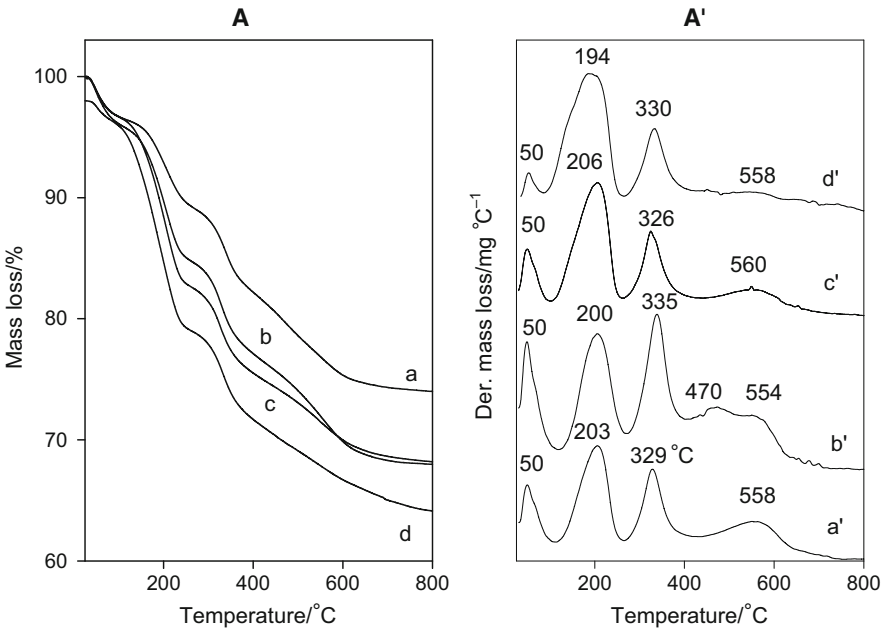

Fig. 5 TG (**A**) and DTG (**A′**) curves of Zr-PCH(X) prepared from zirconium-intercalated clays, *a*, *a′* Zr-PCH(3), *b*, *b′* Zr-PCH(6), *c*, *c′* Zr-PCH(12) and *d*, *d′* Zr-PCH(24)

depends on the Zr contents in the Zr-PCH precursors and reaches a maximum of 21 % for Zr-PCH(24) (Fig. 5A). Simultaneously, the maximum temperature mass loss peaks shifted to lower temperatures, as shown in Fig. 5A', because of the Zr species.

Using Zr-Mt(6) material to prepare Zr-PCH(6) precursors with different amine chain lengths, we noted that the mass loss could be related to the content of amine molecules or to the molecular mass of amine molecules: it varied from 14 % for C_8 amine molecules to 24 % for C_{16} amine molecules. The temperatures where this loss of molecules occurs shift to higher values for C_8 amine molecules and lower values for C_{16} amine molecules. Similar observations were reported for organoclays that were prepared with alkylammonium cations of different alkyl chains [32].

Thermal stability

In situ X-ray diffraction was used for the Zr-Mt(6) sample and Zr-PCH(6) precursors. For Zr-Mt(6), the basal shrank from 2.20 to 1.97 nm and 1.90 nm at 100 and 200 °C, respectively, because of the removal of water molecules, as indicated in the TG studies. Slight change in basal distance from 1.86 to 1.84 nm was observed up to 425 °C (Fig. 6). Qualitatively, the crystallinity of the calcined samples deteriorated as heating temperature was increased. These data were surprising because the intercalated clays were heated generally at temperatures higher than 500 °C to obtain pillared derivatives. However, our study confirmed that a temperature less 500 °C (400 °C) would be enough.

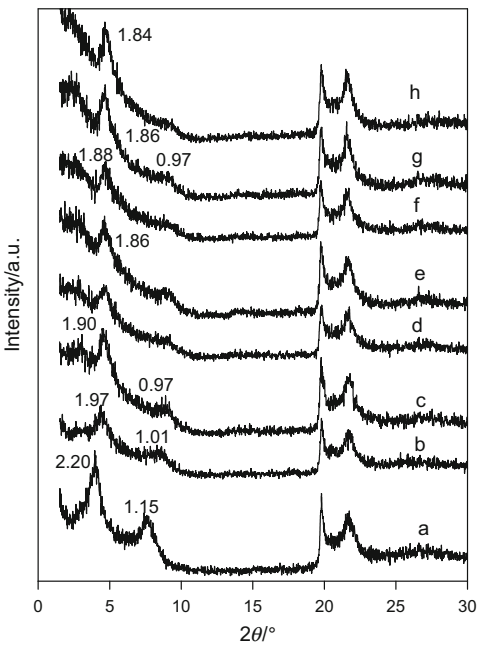

Fig. 6 In situ XRD patterns of *a* Zr-Mt(6) calcined at different temperatures. *b* 100, *c* 200, *d* 250, *e* 300, *f* 350, *g* 400 and *h* 425 °C

The calcinations of different Zr-Mt(X) precursors at 500 °C (reported temperature to obtain pillared zirconia clays) indicate that the pillared clays exhibited an average basal spacing of 1.80 nm for Zr/Clay ratios (X) values higher than 6. However, Zr-Mt(3) did not exhibit a reflection at lower angles because of the poor long-range order of the calcined product. Similar data were reported for zirconia-pillared clays with low zirconium contents [24].

The in situ study of the Zr-PCH(6) precursor is shown in Fig. 7. No variation in basal spacing was observed at heating temperatures below 100 °C. An increase of basal spacing was observed into the range 200–250 °C, from 3.92 to 4.31 nm. This increase was also reported for organoclays [31, 32]. At higher temperatures than 300 °C, continuous shrinkage was observed with less extent at 420 °C, and a value of 3.80 nm was achieved. The decrease is related to the loss of organic amine molecules and dehydroxylation of silica species. This value was maintained until 550 °C with a reflection at a lower angle of 3.81 nm. However, by increasing the temperature to 650 °C and above, the PXRD pattern of Zr-PCH(6) did not exhibit reflections at lower angles, and a reduction of the intensity of the first peak was observed. Similar data were reported in the literature, which can be related to the short-range order in these materials [19, 21] (Fig. 8).

^{29}Si MAS NMR studies

The ^{29}Si MAS NMR technique was used to confirm the incorporation of mesoporous silica in the Zr-PCH materials and identify the local structures of silica species in the materials. The ^{29}Si MAS NMR of the starting Zr-intercalated precursors was reported in our previous studies (supplementary material 1) with an intense resonance peak at −94.2 ppm, which is typical of silicate layers, and Q^3 Si atoms in the tetrahedral coordination and a shoulder at −112.2 ppm, which is related to quartz impurities in the precursors [21, 33]. The similarity between the ^{29}Si MAS NMR of Mt and Zr-Mt(X) confirmed that the intercalation of Zr species did not alter the structural environment of the silicate layers (supporting information 1). However, the ^{29}Si MAS NMR spectra of the Zr-PCH(X) precursors showed different profiles. For example, the Zr-PCH(6) spectrum displayed an intense resonance peak at −110.8 ppm and a weak one at −100.2 ppm. The spectrum did not display the characteristic resonance peak of TEOS at −81.7 ppm [34], which confirms the polycondensation of silicon species [35]. The peaks at −110.8 and −100.2 ppm were assigned to Q^4 Si species Si(SiO4) and Q^3 Si species (HO)(SiO_3), respectively (Fig. 9) [36, 37]. The intensity of the Q^3 Si species of Zr-Mt(6) decreased. (supplementary material 1) These data indicate the presence of silica species in the interlayer space of the clay layers. After calcination at 550 °C, the resonance peak of the Q^4 Si species broadened and shifted to lower values of −108.1 ppm because of the dehydroxylation of the silica species after calcinations [20, 21]. The Q^3 Si band at −94.2 ppm, which is related to the clay layers, was broadened and decreased in intensity with a shift to −92.5 ppm. The band related to Q^3 mesoporous silica remained observable, with a slight shift in position to −100.8 ppm (Fig. 9). Similar ^{29}Si MAS NMR features were obtained when the Zr-PCH(6) precursor was calcined at 650 °C or above; the spectra mainly exhibited a broad resonance peak around −108.1 ppm, which is related to Q^4 Si species with two different shoulders, that is, their

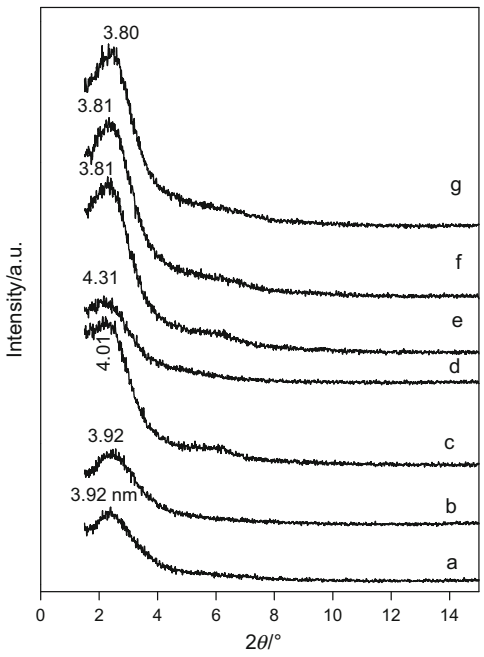

Fig. 7 In situ XRD patterns of *a* Zr-PCH(6) calcined at different temperatures, *b* 100, *c* 200, *d* 250, *e* 300, *f* 350, *g* 400 and *g* 425 °C

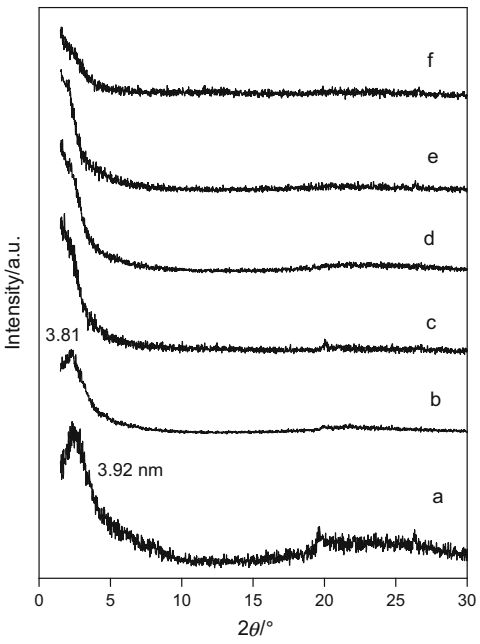

Fig. 8 Powder XRD patterns of *a* Zr-PCH(6) precursor calcined at different temperatures: *b* 550, *c* 650, *d* 750, *e* 850, and *f* 900 °C

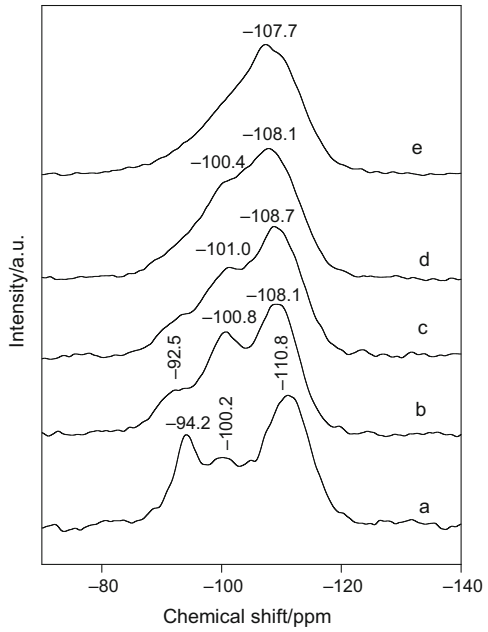

Fig. 9 ^{29}Si MAS NMR spectra of *a* Zr-PCH(6) precursor calcined at different temperatures: *b* 550, *c* 650, *d* 750, and *e* 850 °C

intensities decreased with increasing calcination temperatures. The broadness of the resonance peaks indicates that different silicon species coexisted and were mixed in one phase. It was difficult to identify the other peaks of the clay layers or other silica species, particularly at 850 °C and above (Fig. 9).

The Zr-PCH(X) that was calcined at 550 °C exhibited similar ^{29}Si MAS NMR spectra with an intense peak centered at −108 ppm and a weak peak at −93 ppm, which was assigned to traces of clay layers. The incorporation of Zr species into MCM-41 was deduced from the splitting of the Q^4 Si and Q^3 Si resonance peaks into doublets. In our cases, it was difficult to note this splitting even for higher Zr contents. The large broadness of the peak at −108 ppm caused the difficulty, and the splitting could be embedded in the peak.

Textural properties

The change in the textural properties was evaluated using the N_2 adsorption isotherms. The Zr-Mt(X) precursors had similar N_2 adsorption isotherms with a combination of type I (because of the presence of some micropores) and Type II at relative pressures above 0.5, which are related to the mesoporous character of these precursors. Similar shapes were reported for intercalated clays with other polyoxocations [38]. The amount of adsorbed N_2 at low relative pressures ($P/P_o < 0.1$) increased with the ZrO_2 contents in the precursors. The N_2 gas at a higher relative pressure was enhanced because of the capillary condensation of N_2 gas to N_2 liquid (supplementary material 2).

After the reaction with C_{12} amine molecules and TEOS, the shape of the N_2 adsorption isotherms was unchanged. The Zr-PCH(X) precursors exhibited a type II with slight increase of the N_2 adsorbed, due to the presence of organic molecules around the condensed silica species that blocked the access of N_2 molecules [20] (supplementary material 3). Similar data were reported for conventional PCH and Al-PCH precursors [20, 21]. The removal of C_{12} amine molecules at 550 °C provokes more void space and increases the amount of adsorbed N_2 gas. Indeed, the shape of the isotherms was completely differed from that of the precursors: they exhibited a type II shape, [39] with a hysteresis loop characteristic of type IVa with meso- and macroporosity [40, 41]. The significant increase in the amount of adsorbed N_2 at a low to medium relative pressure indicates an easy accessibility of nitrogen molecules to the micropores and may suggest the presence of supermicropores and small mesopores [39, 41]. N_2 was adsorbed at higher relative pressure because of the capillary condensation, which is associated with the change in pore shapes among the aggregates, as revealed by a change in the hysteresis loop (supplementary material 3).

The textural properties of Zr-PCH(X) materials (after calcinations at 550 °C) are summarized in Table 2. The SSA values were higher than those of the Zr-Mt(X) precursors and depended on the ZrO_2 contents. The lowest value was obtained for Zr-PCH(3) (445 $m^2\ g^{-1}$), whereas the highest value was obtained for Zr-PCH(6) (950 $m^2\ g^{-1}$); the other materials had intermediate values. The obtained values were higher than the reported values for conventional PCH materials [11, 12, 41]. Surprisingly, Zr-PCH(X) exhibited low micropore surface area values, and their percentage to the total SSA was approximately 10–20 %. The total pore volume (TPV) values were also related to the ZrO_2 contents in Zr-PCH(X) materials, with a higher value for the Zr-PCH(6) material. The TPV values were higher than those reported for conventional PCH materials [19, 40]. The average pore diameter (APD) data varied from 3.24 to 3.53 nm, which correspond to pores in the mesopore range and are consistent with the PCH characteristics.

For the Zr-PCH(6) precursor that was calcined at different temperatures, the data are summarized in Table 3. The SSA value decreased with a certain extent when the precursor was calcined at 650 °C. This decrease was accompanied with a reduction of textural properties. The SSA values were further reduced with the raise of the calcination temperature. A noticeable reduction from 950 to 308 $m^2\ g^{-1}$ occurred at 900 °C, which can be associated with the destruction of the clay layers and intercalated silica mesoporous materials, as indicated by a reduction in the TPV value to 0.325 cc g^{-1} and an increase of APD of 4.21 nm. As mentioned in the PXRD paragraph, no reflection peak was detected for the calcined materials;

Table 2 Textural properties of Zr-Mt(X) precursors and their Zr-PCH derivatives after calcinations at 550 °C

Samples	SSA/m^2 g^{-1}	μpore volume/mL g^{-1}	μpore SA/m^2 g^{-1}	TPV/cm^3 g^{-1}	APD/nm
Mt (pure)	78 (180)*	0.002 (0.008)	12 (16)	0.013 (0.028)	6.67 (6.22)
Zr-Mt(3)	231 (445)	0.083 (0.063)	103 (50)	0.194 (0.394)	3.36 (3.53)
Zr-Mt(6)	277 (950)	0.088 (0.104)	122 (142)	0.324 (0.801)	4.67 (3.37)
Zr-Mt(12)	287 (933)	0.095 (0.105)	187 (135)	0.229 (0.818)	3.19 (3.50)
Zr-Mt(24)	318 (908)	0.091 (0.101)	174 (145)	0.320 (0.736)	4.02 (3,24)

* Values between brackets correspond to Zr-PCH materials. SSA corresponds to specific surface area, μpore volume, μpore SS corresponds to micropore surface area TPV corresponds to total pore volume, and APD corresponds to average pore diameter

Table 3 Textural properties of Zr-PCH(6) calcined at different temperatures

Samples	SSA/m^2 g^{-1}	μpore volume/mL g^{-1}	TPV/cm^3 g^{-1}	APD/nm
Zr-PCH(6)	401	0.067	0.287	2.87
550 °C	950	0.104	0.801	3.37
650 °C	808	0.091	0.686	3.40
750 °C	743	0.068	0.652	3.52
850 °C	506	0.059	0.460	3.64
900 °C	308	0.000	0.325	4.21

SSA corresponds to specific surface area, μpore volume corresponds to micropore volume, TPV corresponds to total pore volume, and APD corresponds to average pore diameter

because of the loss of range order and crystallinity. However, the textural properties remained higher and close to those of the PCH materials.

Acidity characterization

Acidity concentration

The measured acid sites of cyclohexylamine are accessible to the probe molecule and are sufficiently strong to interact with the base [10, 18]. The mass loss between 290 and 420 °C was used to estimate the acidity in terms of mmoles of cyclohexylamine.

The TG and DTG curves of desorbed cyclohexylamine on different Zr-Mt(X) that were calcined at 500 °C are shown in Fig. 10A, A'. The pure clay Mt exhibited a maximum temperature peak at 305 °C, The temperature of this peak shifted from 305 to 346 °C for Zr-Mt(X) materials depending on their ZrO_2 content, which is related to the strong interaction between the base molecules and the protonic sites, which were generated by the pillaring zirconia species [18]. A shoulder at 302 °C was also observed and coincided with that of pure Mt clay, which may indicate that some of the cyclohexylamine molecules that were adsorbed on the clay layers contributed to the acidity of these intercalated materials. At a higher ZrO_2 content, the peak became sharp and no shoulders were observed. A broad peak with a lower intensity at 230 °C was also recorded in all of the samples and may be associated with weak acid sites that interact with the base molecules [42]. The peak at lower temperatures (70 °C) is related to the loss of physisorbed water and/or base molecules.

However, the DTG of desorbed cyclohexylamine on Zr-PCH(X) materials exhibited different features with two resolved peaks at maximum temperatures about 200 and 346 °C, which indicates the presence of two types of acid sites with different strengths (Figs. 11A, A') [20, 40]. The peaks at 200 and 342 °C were associated with base molecules that were adsorbed on medium and strong acid sites, respectively. The intensity of the peak at 342 °C was improved with the increase in the ZrO_2 content in the Zr-PCH materials with a slight shift in temperature. Meanwhile, the intensity of the peak at 200 °C decreased for the Zr-PCH materials when the ZrO_2 content increased. The mass loss at lower temperatures, from 25 to 100 °C, which was accompanied with a peak at 70 °C, can be associated with the loss of physisorbed water and the base molecules.

The total acid content of Zr-PCH(X) decreased with the increase in the Zr content in the PCH materials, which is related to the decrease in the number of weak acid sites in the temperature range of 200–310 °C, as shown in Fig. 11, where the area of the DTG peak was reduced. However, the

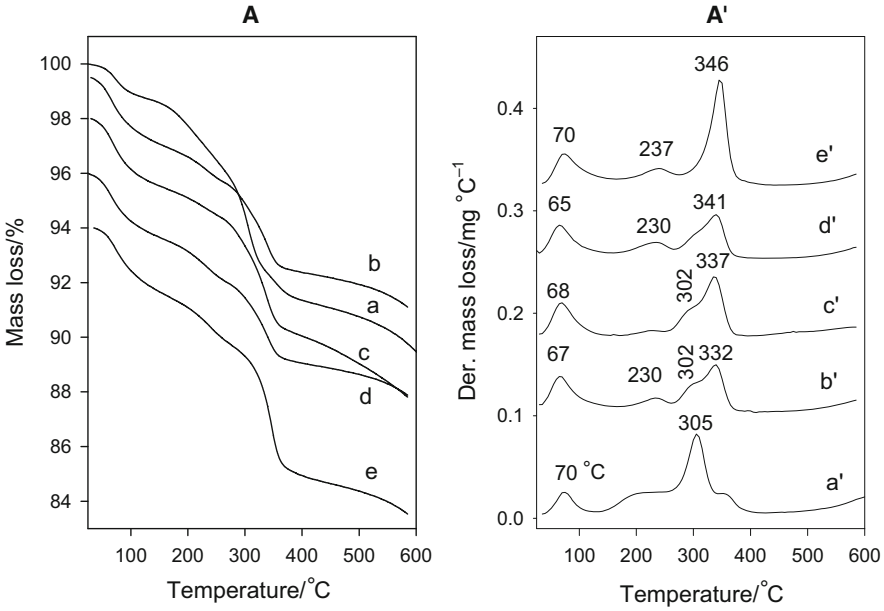

Fig. 10 TG (**A**) and DTG (**A′**) curves of desorbed cyclohexylamine on different Zr-Mt(X) calcined at 500 °C: *a*, *a′* Mt, *b*, *b′* Mt-Zr(3), *c*, *c′* Mt-Zr(6), *d*, *d′* Mt-Zr(12) and *e*, *e′* Mt-Zr(24)

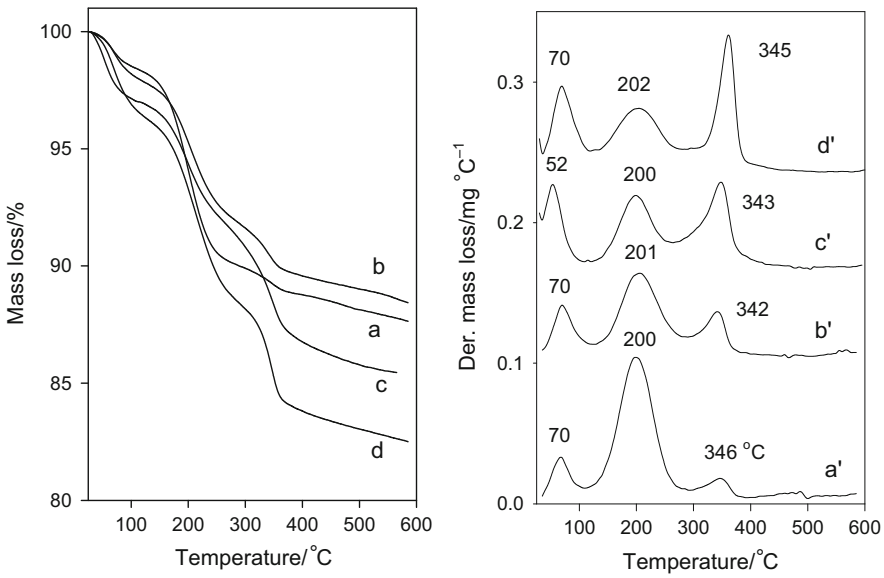

Fig. 11 TG (**A**) and DTG (**A′**) curves of desorbed cyclohexylamine on different Zr-PCH(X) calcined at 550 °C: *a*, *a′* Zr-PCH(3), *b*, *b′* Zr-PCH(6), *c*, *c′* Zr-PCH(12) and *d*, *d′* Zr-PCH(24)

content of medium to strong acid sites increased with the increase in the Zr content (Table 4). The area of the DTG peaks in the temperature range of 310–420 °C was improved with the Zr content (Fig. 11). In comparison with conventional PCH, the increase in the number of acid sites was suggested for the presence of Zr species. The reported values in the table were higher than those reported for Al-PCH materials [20], which can be associated with the difference in the acidity of Al and Zr species and is consistent with the reported data for alumina- and zirconia-pillared clays.

The calcinations temperature also affected the acidity of the Zr-PCH(6) material. Indeed, the Zr-PCH(6) that was calcined at 900 °C exhibited the lowest acidity (0.210 mmol g^{-1}) compared to Zr-PCH(6) calcined at 550 °C (0.993 mmol g^{-1}). Intermediate values were obtained for temperatures in the range of 650–850 °C (Table 4). This difference can be associated with the decrease in the available surface area to the probe molecule or the inaccessibility of acidic sites after calcinations because the layered structure of Zr-PCH materials was destroyed.

Pyridine desorption

The cyclohexylamine probe molecule could not distinguish the different natures of the acid sites. However, the pyridine probe molecule can differentiate between the types of acid sites (Brönsted or Lewis), and their strength character is investigated after the in situ desorption at higher temperatures and in vacuum [43]. The positions of the adsorption bands in the FTIR spectra help to identify the Brönsted and Lewis acid sites.

The raw material (Mt) mainly exhibited weak Lewis acid sites, which were associated with an FTIR adsorption band at 1450 cm^{-1}, after the outgassing temperature at 200 °C and above [38]. Nonetheless, Brönsted acid sites were detected at 1540 cm^{-1} at temperatures below 200 °C. However, the Zr-Mt(6) sample exhibited both Brönsted and Lewis acid sites at temperatures of 300 °C and above, with a relative decrease in the intensity of these bands at 500 °C (Fig. 12). The bands of the Lewis acid sites had higher intensities than those of the Brönsted acid sites [21]. The extent to which pyridine molecules remained adsorbed on the acid sites at higher temperatures reflects both the strength and number of the surface acid sites. From the described results, Zr-Mt(6) appeared to have a Lewis acidic character at temperatures above 200 °C with small amounts of Brönsted acid sites at 500 °C (Fig. 12). The content of ZrO_2 in Zr-Mt(X) affected these observations. At higher contents of ZrO_2 species [samples Zr-Mt(12) and Zr-Mt(24)], an enhancement in the number of Brönsted acid sites and their strength was observed, even at 500 °C. In this case, both bands related to these two types of acid sites were detected in the spectra with better intensity (not shown). However, at a lower ZrO_2 content, the Zr-Mt(3) sample mainly exhibited Lewis acid sites with a FTIR band at 1445 cm^{-1} with a low intensity because of the small amount of weak acid sites. These data are consistent with those in the literature for pillared zirconia clays, and the generation of acid sites in calcined Zr-Mt(X) is associated with the presence of Zr species in the materials [43]. The origin of the acid sites is related to the interaction between zirconium species and the clay layers or to the sites that arise from the hydroxyl groups attached to Zr and the structural hydroxyl groups in the pillared clays [44].

In the case of Zr-PCH(X) materials with X values higher or equal to 6, the pyridine desorption spectra exhibited clear bands that are related to Brönsted and Lewis acid sites at 1445 and 1545 cm^{-1}, respectively. An intense additional absorption band at 1490 cm^{-1}, which is associated with both acid sites, was also observed [29]. The intensity of these bands slightly decreased, even at outgassing temperatures of 300 °C (Fig. 12). At 500 °C, the materials exhibited Brönsted and Lewis characteristics. These data are related to an improvement in the number of acid sites and their strength nature (Fig. 12). At a low ZrO_2 content in the Zr-PCH(3) material, different results were obtained at 300 °C; however, the characteristic bands of B and L sites were detected with low intensity. The lower intensity of the band at 1490 cm^{-1} indicates a smaller contribution of Brönsted acid sites to this band. At higher temperatures, the band at 1490 cm^{-1} reduced because of the weakness of the Brönsted acid sites and strength of the Lewis acid sites (no shown). The conventional PCH material with pure silica exhibited a notably similar behavior of the Zr-PCH(3) material with a Lewis character at 300 °C [45].

Pure zirconium oxide (ZrO_2) exhibited mainly Lewis acid sites at 300 °C, and pure mesoporous silica also exhibited a Lewis character with a different strength [46, 47]. In our case, the combination of these two species and their interaction with the clay layers generated stronger Brönsted acid sites than a mixture of ZrO_2–SiO_2 species. Similar data were reported for Zr-PCH materials that were prepared from a pure layered silicate magadiite [48].

Table 4 Acidity concentration of starting Zr-Mt(X) and their resulting Zr-PCH(X) calcined at 550 °C

Samples	Total acidity[a]	Weak acidity[a] (120–310 °C)	Strong acidity[a] (310–420 °C)
Mt	0.057[a]	0	0.057
Zr-Mt(3)	0.326[a] (1.031)	0 (0.910)	0 (0.121)
Zr-Mt(6)	0.367[a] (0.993)	0 (0.802)	0 (0.191)
Zr-Mt(12)	0.386[a] (0.973)	0 (0.739)	0 (0.234)
Zr-Mt(24)	0.394[a] (0.953)	0 (0.656)	0 (0.297)
Zr-PCH(6)650	0.812	0.676	0.135
Zr-PCH(6)750	0.652	0.581	0.101
Zr-PCH(6)850	0.433	0.380	0.053
Zr-PCH(6)900	0.120	0.120	0

The values between brackets correspond to those Zr-PCH(X) materials after calcinations at 550 °C

[a] Corresponds to mmole of acid sites g^{-1} of sample

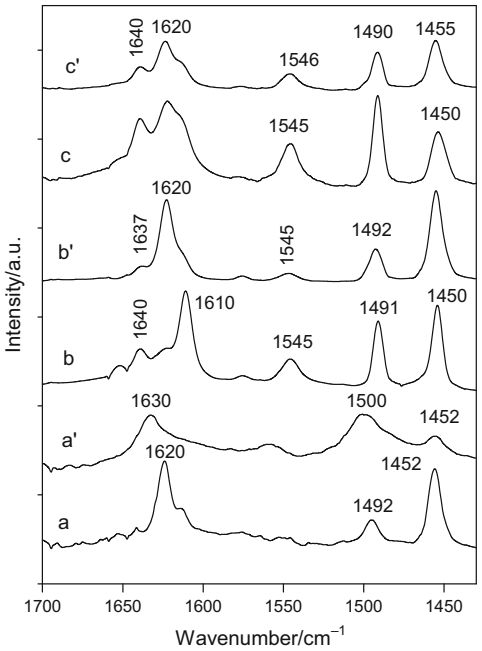

Fig. 12 FTIR spectra of pyridine desorbed at 300 °C in vacuum on different materials. *a* Mt, *b* MtZr(6) and *c* Zr-PCH(6). *a*′, *b*′, *c*′ correspond to pyridine desorbed at 500 °C

Conclusions

Porous clay heterostructures were successfully prepared from a zirconium-intercalated clay mineral. The intercalation of Zr species between the clay sheets plays a major role in the preparation of PCH materials. The physicchemical properties of these materials were affected by different factors, such as the content of zirconium species in the starting precursors, length of the alkyl chain used during the preparation and calcination temperatures of the resulting PCH materials. The prepared precursors exhibited good thermal stability up to 600 °C with higher specific surface areas and larger pore volumes than the conventional PCH materials, and approximately 20 % of the microporosity was maintained. The presence of zirconium species also affected the loss temperature of the surfactants and generated two types of acid sites with different strengths, as indicated by the TG-DTG desorption of the cyclohexylamine probe molecule. The concentration of weak to medium acid sites decreased and that of strong acid sites was improved with the increase in the Zr/Si molar ratios in Zr-PCHs. The strong Brönsted acid sites were also associated with the presence of zirconium species at the desorption temperatures of pyridine at temperatures above 400 °C. This method of synthesis enables us to tune some of the important properties that can be used in different catalytic applications.

References

1. Vallet-Regi M, Balas F, Arcos D. Mesoporous materials for drug delivery. Angew Chem Int Ed. 2007;46:7548–56.
2. Bhattacharyya S, Lelong G, Saboungi ML. Recent progress in the synthesis and selected applications of MCM-41: a short review. J Exp Nanosci. 2006;1:375–95.
3. Raman NK, Anderson MT, Brinker CT. Template-based approaches to the preparation of nanoporous silicas. Chem Mater. 1996;8:1682–701.
4. Galarneau A, Barodawalla A, Pinnavaia TJ. Porous clay heterostructures formed by gallery-templated synthesis. Nature. 1994;374:529–31.
5. Pires J, Pinto M, Estella J, Echeverría JC. Characterization of the hydrophobicity of mesoporous silicas and clays with silica pillars by water adsorption and DRIFT. J Colloid Interface Sci. 2008;317:206–13.
6. Chmielarz L, Kuśtrowski P, Drozdek M, Dziembaj R, Cool P, Vansant EF. Selective catalytic oxidation of ammonia into nitrogen over PCH modified with copper and iron species. Catal Today. 2006;114:319–25.
7. Arellano-Cárdenas S, Gallardo-Velázquez T, Osorio-Revilla G, López-Cortez M. Preparation of a porous clay heterostructure and study of its adsorption capacity of phenol and chlorinated phenols from aqueous solutions. Water Environ Res. 2008;80:60–7.
8. Srithammaraj K, Magaraphan R, Manuspiya H. Modified porous clay heterostructures by organic–inorganic hybrids for nanocomposite ethylene scavenging/sensor packaging film. Packag Technol Sci. 2012;25:63–72.
9. Gârea SA, Mihai AI, Ghebaur A, Nistor C, Sârbu A. Porous clay heterostructures: a new inorganic host for 5-fluorouracil encapsulation. Int J Pharm. 2015;491:299–309.
10. Kooli F, Hian PC, Weirong Q, Alshahateet SF, Chen F. Effect of the acid activated clays on the properties of porous clay heterostructures. J Porous Mater. 2006;13:319–24.
11. Chmielarz L, Piwowarska Z, Kuśtrowski P, Gil B, Adamski A, Dudek B, Michalik M. Porous clay heterostructures (PCHs) intercalated with silica-titania pillars and modified with transition metals as catalysts for the DeNOx process. Appl Catal B Environ. 2009;91:449–59.
12. Polverejan M, Liu Y, Pinnavaia TJ. Aluminated derivatives of porous clay heterostructures (PCH) assembled from synthetic saponite clay: properties as supermicroporous to small mesoporous acid catalysts. Chem Mater. 2002;14:2283–8.
13. Pinto ML, Saini VK, Guil JM, Pires J. Introduction of aluminum to porous clay heterostructures to modify the adsorption properties. Appl Clay Sci. 2014;101:497–502.
14. Chmielarz L, Gil B, Kustrowski P, Piwowarska Z, Dudek B, Michalik M. Montmorillonite-based porous clay heterostructures (PCHs) intercalated with silica–titania pillars—synthesis and characterization. J Solid State Chem. 2009;182:1094–104.
15. Cecilia JA, García-Sancho C, Franco F. Montmorillonite based porous clay heterostructures: influence of Zr in the structure and acidic properties. Microporous Mesoporous Mater. 2013;176:95–102.
16. Yamaguchi T. Application of ZrO_2 as a catalyst and a catalyst support. Catal Today. 1994;20:199–217.
17. Ohtsuka K. Preparation and properties of two-dimensional microporous pillared interlayered solids. Chem Mater. 1997;9:2039–50.
18. Kooli F, Jones W. Systematic comparison of a saponite clay pillared with Al and Zr metal oxides. Chem Mater. 1997;9:2913–20.

19. Pinto ML, Marques J, Pires J. Porous clay heterostructures with zirconium for the separation of hydrocarbon mixtures. Sep Purif Technol. 2012;98:337–43.
20. Kooli F. Porous clay heterostructures (PCHs) from Al_{13}-intercalated and Al_{13}-pillared montmorillonites: properties and heptane hydro-isomerization catalytic activity. Microporous Mesoporous Mater. 2014;184:184–92.
21. Kooli F, Yan L, Hbaieb K, Al-Faze R. Characterization and catalytic properties of porous clay heterostructures from zirconium intercalated clay and its pillared derivatives. Microporous Mesoporous Mater. 2016;226:482–92.
22. Kooli F, Sim TH, Jian D, Yan L, Alshahateet SF, Martin C, Rivers V. Zirconium nitrate solution as pillaring agent of montmorillonites clays. Clay Sci. 2006;12(2):301–5.
23. Awate SV, Waghmode SB, Patil KR, Agashe MS, Joshi PN. Influence of preparation parameters on characterization of zirconia-pillared clay using ultrasonic technique and its catalytic performance in phenol hydroxylation reaction. Korean J Chem Eng. 2001;18:257–62.
24. Toranzo R, Vicente MV, Banares-Munoz MA, Gandı LM, Gil A. Pillaring of saponite with zirconium oligomers. Microporous Mesoporous Mater. 1998;173:173–88.
25. Kooli F, Jones W. Al and Zr pillared acid-activated saponite clays: characterization and properties. J Mater Chem. 1998; 8:2119–24.
26. Farfan EM, Sham E, Grange P. Pillared clay: preparation and characterization of zirconium pillared montmorillonite. Catal Today. 1992;15:515–26.
27. Cool P, Vansant EF. Preparation and characterization of zirconium pillared laponite and hectorite. Microporous Mater. 1996;6: 27–36.
28. Bahranowski K, Włodarczyk W, Wisła-Walsh E, Gaweł A, Matusik J, Klimek A, Gil B, Michalik-Zym A, Dula R, Socha RP, Serwicka EM. [Ti, Zr]-pillared montmorillonite—a new quality with respect to Ti- and Zr-pillared clays. Microporous Mesoporous Mater. 2015;202:155–64.
29. Ursu AV, Jinescu G, Gros F, Nistor ID, Miron ND, Lisa G, Silion M, Djelveh G, Azzouz A. Thermal and chemical stability of Romanian bentonite. J Therm Anal Calorim. 2011;106: 965–71.
30. Sun Kou MR, Mendioroz S, Guijarro MI. A thermal study of Zr-pillared montmorillonite. Themochim Acta. 1998;323:145–57.
31. Kooli F, Liu Y, Tan SX, Zheng J. Organoclays from alkaline-treated acid-activated clays. J Therm Anal Calorim. 2014;115: 1465–75.
32. Zhu J, Shen W, Ma Y, Zhou Q, Yuan P, Liu D, He H. The influence of alkyl chain length on surfactant distribution within organo-montmorillonites and their thermal stability. J. Thermal Anal Calorim. 2016;109:301–9.
33. He H, Duchet J, Galy J, Gerard JF. Grafting of swelling clay materials with 3-aminopropyltriethoxysilane. J Colloid Interface Sci. 2005;288:171–6.
34. Belver C, Aranda P, Martin-Luengo MA, Ruiz-Hitzky E. New silica/alumina–clay heterostructures: properties as acid catalysts. Microporous Mesoporous Mater. 2012;147:157–66.
35. Wang F, Nimmo SL, Cao B, Mao C. Oxide formation on biological nanostructures via a structure-directing agent: towards an understanding of precise transcription. Chem Sci. 2012;3: 2639–45.
36. Zapata PA, Belverb C, Quijada R, Aranda P, Ruiz-Hitzky E. Silica/clay organo-heterostructures to promote polyethylene–clay nanocomposites by in situ polymerization. Appl Catal A Gen. 2013;453:142–50.
37. Zimowska M, Pálková H, Madejová J, Dula R, Pamin K, Olejniczak Z, Gil B, Serwicka EM. Laponite-derived porous clay heterostructures: III. The effect of alumination. Microporous Mesoporous Mater. 2013;175:67–75.
38. Kooli F. Pillared montmorillonites from unusual antiperspirant aqueous solutions: characterization and catalytic tests. Microporous Mesoporous Mater. 2013;167:228–36.
39. Benjelloun M, Cool P, Linssen T, Vansant EF. Acidic porous clay heterostructures: study of their cation exchange capacity. Microporous Mesoporous Mater. 2001;49:83–94.
40. Pichowicz M. Mokaya. R. Porous clay heterostructures with enhanced acidity obtained from acid-activated clays. Chem Commun. 2001;20:2100–1.
41. Wang Y, Lin X, Wen K, Zhu J, He H. Effects of organic templates on the structural properties of porous clay heterostructures: a non-micellar template model for porous structure. J Porous Mater. 2015;22:219–28.
42. Breen C. Thermogravimetric study of the desorption of cyclohexylamine and pyridine from an acid-treated Wyoming bentonite. Clay Miner. 1991;26:473–86.
43. Bagshaw SA, Cooney RP. FTIR surface site analysis of pillared clays using pyridine probe species. Chem Mater. 1993;5:1101–9.
44. Lambert JF, Poncelet G. Acidity in pillared clays: origin and catalytic manifestations. Top Catal. 1997;11:43–56.
45. Wei L, Tang T, Huang B. Novel acidic porous clay heterostructure with highly ordered organic–inorganic hybrid structure: one-pot synthesis of mesoporous organosilica in the galleries of clay. Microporous Mesoporous Mater. 2004;67: 175–9.
46. Cavani F, Guidetti S, Marinelli L, Piccinini M, Chedini E, Signoretto M. The control of selectivity in gas-phase glycerol dehydration to acrolein catalysed by sulfated zirconia. Appl Catal B. 2010;100:197–204.
47. Carriazo D, Domingo C, Martin C, Rives V. PMo or PW heteropoly acids supported on MCM-41 silica nanoparticles: characterisation and FT-IR study of the adsorption of 2-butanol. J Soild State Chem. 2008;181:2046–57.
48. Ma Y, Sun H, Sun Q, Zhang H. Zirconium-doped porous magadiite heterostructures upon 2D intragallery in situ hydrolysis–condensation–polymerization strategy for liquid-phase benzoylation. RSC Adv. 2015;5:67853–65.